Editors' Suggestion

# Measurements of Capacitive Coupling Within a Quadruple-Quantum-Dot Array

Samuel F. Neyens,[1,*] E.R. MacQuarrie,[1] J.P. Dodson,[1] J. Corrigan,[1] Nathan Holman,[1] Brandur Thorgrimsson,[1] M. Palma,[1] Thomas McJunkin,[1] L.F. Edge,[2] Mark Friesen,[1] S.N. Coppersmith,[1,3] and M.A. Eriksson[1]

[1] *University of Wisconsin-Madison, Madison, Wisconsin 53706, USA*
[2] *HRL Laboratories, LLC, 3011 Malibu Canyon Road, Malibu, California 90265, USA*
[3] *University of New South Wales, Sydney, Australia*

(Received 22 July 2019; revised manuscript received 19 November 2019; published 23 December 2019)

We present measurements of the capacitive coupling energy and the interdot capacitances in a linear quadruple-quantum-dot array in undoped Si/SiGe. With the device tuned to a regime of strong (>1 GHz) intra-double-dot tunnel coupling, as is typical for double-dot qubits, we measure a capacitive coupling energy of $20.9 \pm 0.3$ GHz. In this regime, we demonstrate a fitting procedure to extract all the parameters in the four-dimensional Hamiltonian for two capacitively coupled charge qubits from a two-dimensional slice through the quadruple-dot charge-stability diagram. We also investigate the tunability of the capacitive coupling energy, using interdot barrier gate voltages to tune the inter- and intra-double-dot capacitances, and change the capacitive coupling energy of the double dots over a range of 15–32 GHz. We provide a model for the capacitive coupling energy based on the electrostatics of a network of charge nodes joined by capacitors, which shows how the coupling energy should depend on inter-double-dot and intra-double-dot capacitances in the network, and find that the expected trends agree well with the measurements of coupling energy.

DOI: 10.1103/PhysRevApplied.12.064049

## I. INTRODUCTION

Electron spins in semiconductor quantum dots are a promising platform for quantum computation [1–3]. Quantum dots formed in Si/SiGe heterostructures have many advantages, including high electron mobility, low natural abundance of spinful isotopes in Si, and compatibility with industrial Si-based fabrication techniques [4]. Such devices were initially realized in doped heterostructures [5], but the transition to undoped, fully gated structures [6–9] has led to improved charge stability. Undoped Si/SiGe heterostructures have now hosted many qubit architectures, with recent demonstrations of single-dot qubits such as the Loss-DiVincenzo qubit [10–15]; double-dot qubits such as the singlet-triplet qubit [9,16,17], quantum-dot hybrid qubit (QDHQ) [18,19], and valley qubit [20,21]; and triple-dot qubits such as the exchange-only qubit [22].

Two-qubit gates in semiconductor quantum dots have been demonstrated through use of the exchange coupling in Loss-DiVincenzo qubits [12,13,15,23–26] and through use of the capacitive coupling in singlet-triplet qubits [27,28] and charge qubits [29]. For double-dot qubits, the capacitive interaction arises when the individual qubit states, $|0\rangle$ and $|1\rangle$, have different admixtures of the eigenstates of electron position, $|L\rangle$ and $|R\rangle$. This difference can be described as an effective dipole moment for each qubit, leading to a dipole-dipole interaction between the qubits. The maximum such interaction energy between two double-dot qubits is equal to the shift in detuning experienced by one double-dot qubit owing to the complete transfer of an electron between dots in the neighboring qubit. This interaction energy can be obtained by measuring the shift in the polarization line of one double dot owing to a change in polarization of the other double dot [30–33]. The resulting energy shift is the coupling term $g$ in the Hamiltonian for two double-dot qubits that interact capacitively. We refer to this energy from here on as the capacitive coupling.

In this work, we report measurements of the capacitive coupling in a quadruple-quantum-dot device in undoped Si/SiGe. We tune the device to a regime of strong intra-double-dot tunnel coupling ($t > 1$ GHz in both double dots), to match the conditions of typical double-dot qubit experiments, and measure the capacitive coupling to be $20.9 \pm 0.3$ GHz. In this regime, we demonstrate a fitting procedure with which we obtain, from a two-dimensional (2D) slice through the quadruple-dot charge-stability diagram, all the parameters in the four-dimensional (4D) Hamiltonian for capacitively coupled charge qubits. We

*neyens@wisc.edu

 

investigate the tunability of the capacitive coupling *in situ*, using barrier gate voltages to change the inter-double-dot (inter-DD) and intra-double-dot (intra-DD) capacitances in the quadruple-dot array, and find the capacitive coupling changes over a range of 15–32 GHz, in a way that trends positively with inter-DD capacitance and negatively with intra-DD capacitances. We interpret the range of interdot capacitances observed here in terms of changes in interdot spacing and estimate that the changes we make to the barrier gate voltages shift the positions of the quantum dots by tens of nanometers. We provide a simple model based on the electrostatics of a system of charge nodes joined by capacitors to illustrate how the capacitive coupling should depend on inter-DD and intra-DD capacitances, and we find that the expected trends from the model agree well with the trends in the measured data.

## II. RESULTS AND DISCUSSION

### A. Fabrication and measurement

The device we study is composed of six quantum dots, four arrayed linearly in the main channel and two in separate channels used to sense the electron occupation of the array. A false-colored SEM micrograph of a lithographically identical device is shown in Fig. 1(a). The device is an accumulation-mode overlapping gate device with three layers, one each for screening, accumulation, and tunnel barrier control (see the Supplemental Material

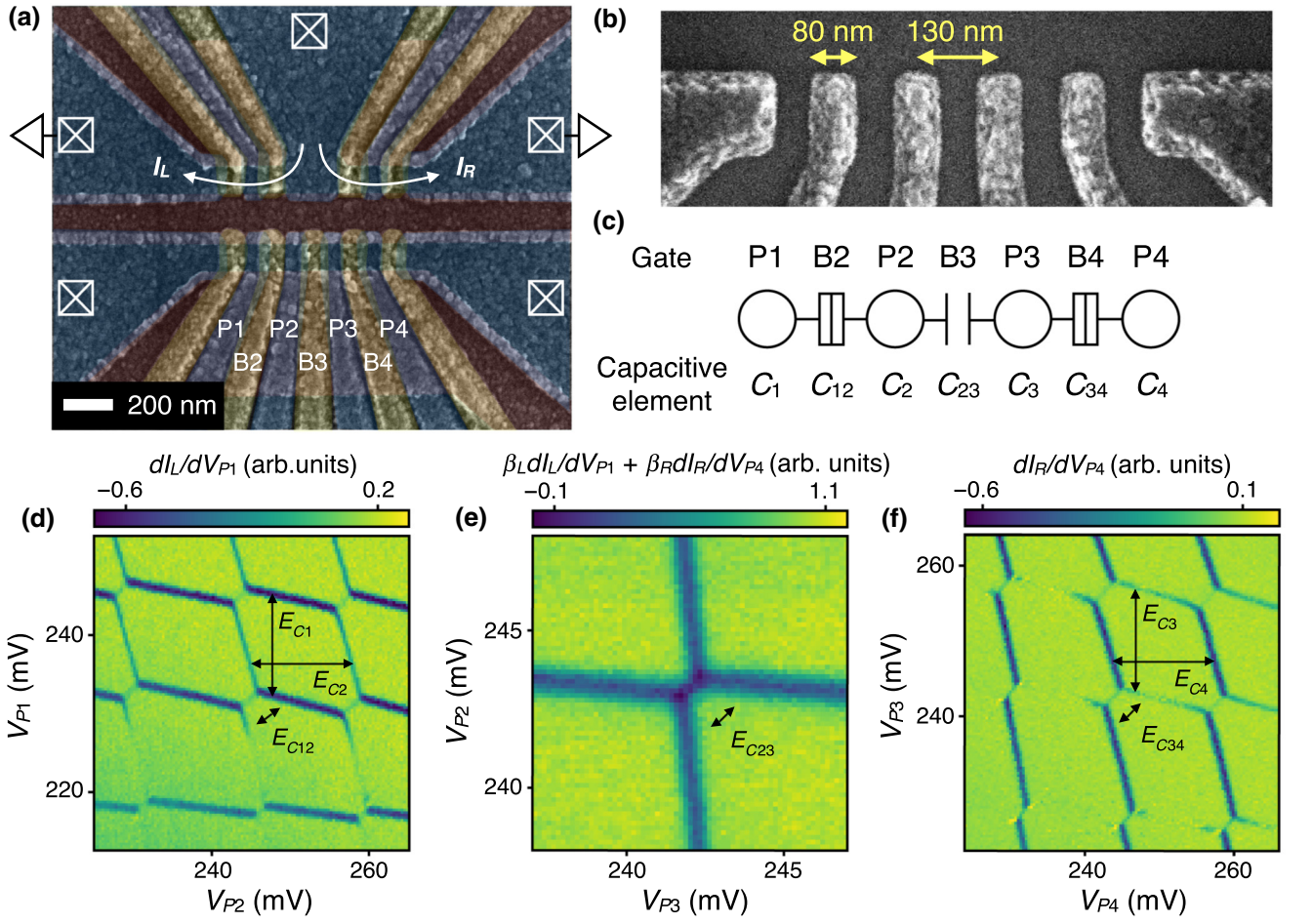


FIG. 1. (a) False-colored SEM micrograph of a device lithographically identical to the device measured here. Plunger (P) and barrier (B) gates used in the tuning of the four-dot array are labeled. The charge-sensor currents $I_L$ and $I_R$ are also labeled. (b) Higher-magnification image of the accumulation-layer pattern showing the dimensions of the plunger gate array. (c) Schematic of the model of the four-dot array as a network of charge nodes and capacitors. Here $C_i$ is the sum of capacitances to dot $i$, and $C_{ij}$ is the capacitance between dots $i$ and $j$. Capacitances to reservoirs and gates are not shown. (d)–(f) Charge-stability diagrams for each nearest-neighbor pair of dots in the array. The indicated energy scales correspond to the dot charging energies $E_{C_i}$ and the electrostatic coupling energies $E_{C_{ij}}$. Here $E_{C_i}$ range from 2.4 to 4.4 meV, and $E_{C_{ij}}$ range from 120 to 680 $\mu$eV, depending on the tuning. The data shown in (e) are a weighted sum of transconductance signals from the two charge-sensor amplifiers: $\beta_L dI_L/dV_{P1} + \beta_R dI_R/dV_{P4}$, where $\beta_{L(R)}^{-1}$ is the range of the signal from the left (right) amplifier. Here $\beta_L = 1.9 \times 10^4$ and $\beta_R = 78$. The difference in signal range is due to the difference in amplification schemes for the two charge sensors, as described in the main text.

[34–36] for further details). Quantum-dot chemical potentials and interdot barrier potentials are primarily controlled by the plunger (P) and barrier (B) gates, respectively. The plunger gates are 80 nm wide with 130 nm pitch, as shown in a higher-magnification image of the accumulation-layer pattern in Fig. 1(b).

Measurements are performed in a dilution refrigerator with a base temperature below 20 mK. The device is tuned to form a quantum dot under each plunger gate in the main channel, resulting in a linear array of four quantum dots. Two quantum dots are also formed in the auxiliary channels as charge sensors, with the left (right) charge sensor mostly sensitive to double dot 1–2 (3–4). The left charge sensor is connected to a cryogenic amplifier similar to that in Ref. [37]; the right charge-sensor current is amplified only at room temperature. Measurements of the charge occupation of the four-dot array are performed by modulating a plunger gate above each double dot and measuring the charge-sensor currents with lock-in amplifiers at those modulation frequencies. The quantum dots are set to desired electron occupations by finding the last electron transitions in the dots and then counting up on the charge-stability diagram. The tunnel couplings between dots are controlled with barrier gate voltages. Here $V_{B2}$ and $V_{B4}$ are generally tuned to be much more positive than $V_{B3}$ so that the tunnel couplings within each double dot are large whereas the tunnel coupling between the double dots is negligible. Thus, the significant coupling between the double dots is capacitive. We note that during the experiments described below (e.g., those in Sec. II C) no compensating voltages on barriers to reservoirs were necessary to maintain the tunnel rates to source and drain in the range needed for the measurements.

Figure 2 shows a measurement of the capacitive coupling between the double dots. This measurement is done by measuring a 2D slice through the 4D quadruple-dot charge-stability diagram. By simultaneously sweeping the detuning of both double dots, we observe the shift in the polarization line of each double dot owing to the change in polarization of the other double dot. The magnitude of the shift is extracted by fitting line cuts of each polarization line, finding the center point in each line cut, and fitting the curve describing the shift of the center points in detuning space. The functional form used to fit this curve is a hyperbolic tangent (tanh), based on the expected form for the polarization of a double dot as a function of its detuning [38]. The amplitude of this tanh function in units of detuning energy, indicated by the arrows in Fig. 2, is equal to the capacitive coupling $g$, which for the measurement in Fig. 2 is found to be $28.4 \pm 0.4$ GHz.

At each tuning of the barrier gate voltages, the detuning lever arms for both double dots are measured by sweeping the temperature and measuring the broadening of the polarization lines [39], which also enables an extraction of the electron temperature $T_e = 155$ mK. We also measure

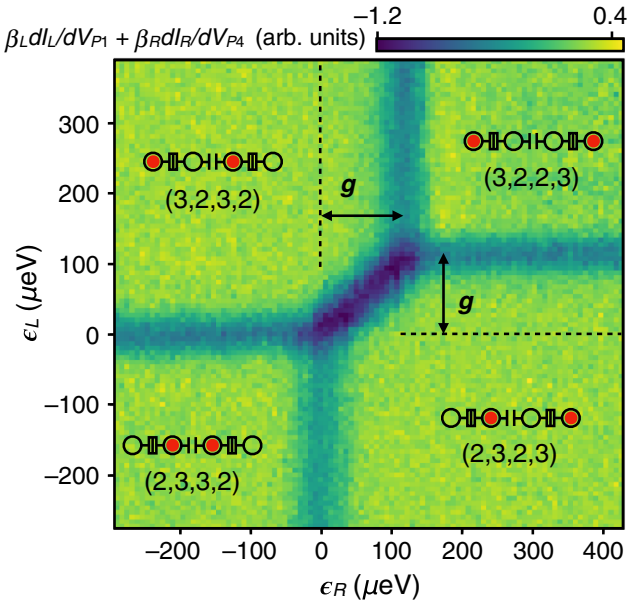


FIG. 2. Measurement of the capacitive coupling energy between two double dots from the shift of the polarization line. The arrows indicate the magnitude of the polarization line shift, and the dashed lines indicate where the lines would be for $g = 0$. For this dataset, $g = 28.4 \pm 0.4$ GHz. Here $V_{P1}$ ($V_{P4}$) is used to sweep $\epsilon_L$ ($\epsilon_R$). The data shown are a weighted sum of transconductance signals from the two charge-sensor amplifiers: $\beta_L dI_L/dV_{P1} + \beta_R dI_R/dV_{P4}$, with $\beta_L = 1.6 \times 10^4$ and $\beta_R = 68$.

the individual capacitive elements of the quadruple-dot system, shown schematically in Fig. 1(c), including $C_i$, the total capacitance to dot $i$, and $C_{ij}$, the capacitance between dots $i$ and $j$. These capacitances are obtained from the corresponding self-charging energies $E_{C_i}$ and electrostatic coupling energies $E_{C_{ij}}$, which can be read from the charge-stability diagrams by the dimensions labeled in Figs. 1(d)–1(f) [34].

The double dots are both tuned to be near the (3,2)-(2,3) polarization line, which is the charge qubit regime with the first valley shell filled in all dots. Using this electron configuration enables the detection of transitions of the inner two dots (2 and 3), which is necessary to measure the electrostatic energies indicated in Figs. 1(d)–1(f). As these dots are not coupled directly to reservoirs, their transitions require cotunneling through the outer dots (1 and 4), the rate of which becomes suppressed when the outer dots are empty and their chemical potentials lie well above the chemical potentials of the inner dots [40].

### B. Capacitive coupling at strong interdot tunnel couplings

The capacitive coupling measurement shown in Fig. 2 is taken with low intra-DD tunnel couplings. From lack of tunnel broadening of the polarization lines, we determine $t_{12}, t_{34} < k_B T_e$ for that measurement, where $k_B T_e \sim 3$ GHz.

Suitable values of the tunnel couplings and the capacitive coupling are important for enabling high-fidelity single- and two-qubit gates. To enable good single-qubit control, the intra-DD tunnel couplings should typically be of the order of 1–10 GHz between dots in charge [41–43], singlet-triplet [9,16], quantum-dot hybrid [18,19,44], and valley [20,21] qubits. Furthermore, to couple the qubits purely capacitively, the tunnel rate between dots 2 and 3 should be low so that the exchange coupling between dots 2 and 3 is negligible and the probability of state leakage across B3 during control and readout of the qubits is low.

Taking these considerations into account, we look at an example configuration with strong intra-DD tunnel coupling and weak inter-DD tunnel coupling and measure the capacitive coupling of the system. We set $V_{B3}$ to achieve a low inter-DD tunneling rate $t_{23} \lesssim 1$ kHz, measured by varying the lock-in frequency and tracking the visibility of the polarization line between dots 2 and 3. We raise $V_{B2}$ and $V_{B4}$ until $t_{12}, t_{34} > k_B T_e$, determined by observing tunnel broadening of the intra-DD polarization lines. In this regime, we measure $g = 20.9 \pm 0.3$ GHz. This is reduced compared with the measurement with weaker intra-DD tunnel coupling shown in Fig. 2, where $g = 28.4 \pm 0.4$ GHz, but is still expected to be strong enough to perform high-fidelity two-qubit gates for QDHQs [45].

Figure 3(a) shows a 2D slice of the quadruple-dot stability diagram at this configuration. As explained above, the shift of the polarization lines in energy corresponds to the magnitude of the capacitive coupling. In addition, at this tuning where intra-DD tunnel couplings are high, each shifted polarization line acquires an increased curvature owing to the tunnel broadening of the opposite polarization line. By adopting a more sophisticated model that incorporates the effects of tunnel coupling, electron temperature, and capacitive coupling, we can fit this curvature to extract more information about the Hamiltonian of the quadruple-dot system. Using this analysis, the 2D dataset shown in Fig. 3(a) yields all the parameters in the Hamiltonian for two coupled charge qubits in the absence of noise, given a known detuning lever arm. The procedure is as follows. We write the 4D Hamiltonian,

$$H = \frac{\epsilon_L}{2}\sigma_z \otimes I + t_L \sigma_x \otimes I + \frac{\epsilon_R}{2} I \otimes \sigma_z + t_R I \otimes \sigma_x + \frac{g}{4}(I - \sigma_z) \otimes (I - \sigma_z), \quad (1)$$

where $\epsilon_{L(R)}$ is the detuning in the left (right) double dot, $t_{L(R)} = t_{12(34)}$, $g$ is the capacitive coupling, $I$ is the identity operator, and $\sigma_i$ are the usual Pauli operators. From $H$, we obtain the eigenstates $|\psi_i\rangle$ as functions of $\epsilon_L$, $\epsilon_R$, $t_L$, $t_R$, and $g$. Then, extending the method in Ref. [38] to a two-qubit system, we calculate the expectation value of the charge polarization of each double dot, averaged over a Maxwell-Boltzmann distribution:

$$P_{L(R)}(\epsilon_L, \epsilon_R; t_L, t_R, g) = \frac{1}{Z}\sum_{i=1}^{4} \langle \psi_i | \sigma_z^{L(R)} | \psi_i \rangle e^{-E_i/k_B T_e}, \quad (2)$$

where $\sigma_z^L = \sigma_z \otimes I$, $\sigma_z^R = I \otimes \sigma_z$, and $Z$ is the partition function. This expression yields two functions, one for the charge polarization of each double dot as a function of $\epsilon_L$ and $\epsilon_R$ and parametrized by $t_L$, $t_R$, and $g$. Fitting each of these functions to the shifted polarization line data in Fig. 3(a) yields the theoretical stability diagram shown in Fig. 3(b) [34]. From the fit we extract the parameters $t_L = 5.8 \pm 0.4$ GHz, $t_R = 7.0 \pm 0.5$ GHz, and $g = 20.9 \pm 0.3$ GHz, allowing us to write out the complete 4D Hamiltonian for coupled charge qubits at every point in Fig. 3(a).

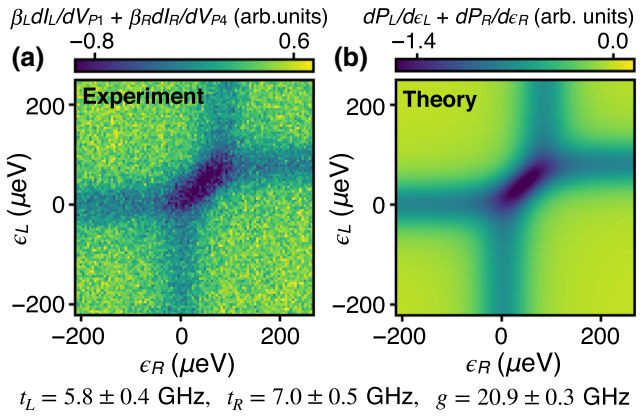


FIG. 3. (a) A 2D slice through the quadruple-dot stability diagram, taken using $V_{P1}$ ($V_{P4}$) to sweep $\epsilon_L$ ($\epsilon_R$), with $t_{23} \lesssim 1$ kHz and $t_{12}, t_{34} > k_B T_e$. The data shown are a weighted sum of transconductance signals from the two charge-sensor amplifiers, with $\beta_L = 4.0 \times 10^4$ and $\beta_R = 1.4 \times 10^2$. (b) A theoretical fit to the data based on the 4D Hamiltonian for two coupled charge qubits. Hamiltonian parameters extracted from the fit are listed at the bottom.

### C. Controlling the capacitive coupling with barrier gate voltages

Comparison of the measurements in Fig. 2 and Fig. 3(a) shows how a change of barrier gate voltages that increases the intra-DD tunnel couplings results in a significant decrease in the capacitive coupling (around 25%). We further investigate the tunability of the capacitive coupling in response to the barrier gate voltages $V_{B2}$, $V_{B3}$, and $V_{B4}$, by measuring the coupling energy as well as all the parameters of the capacitance network shown in Fig. 1(c) as a function of these voltages.

Figure 4 shows the results of the measurements, where we observe a range of capacitive couplings from 15 to 32 GHz in response to changes in interdot barrier gate voltages. Each of these barrier gate voltages tunes the capacitance between the dots straddling that barrier. In this way,

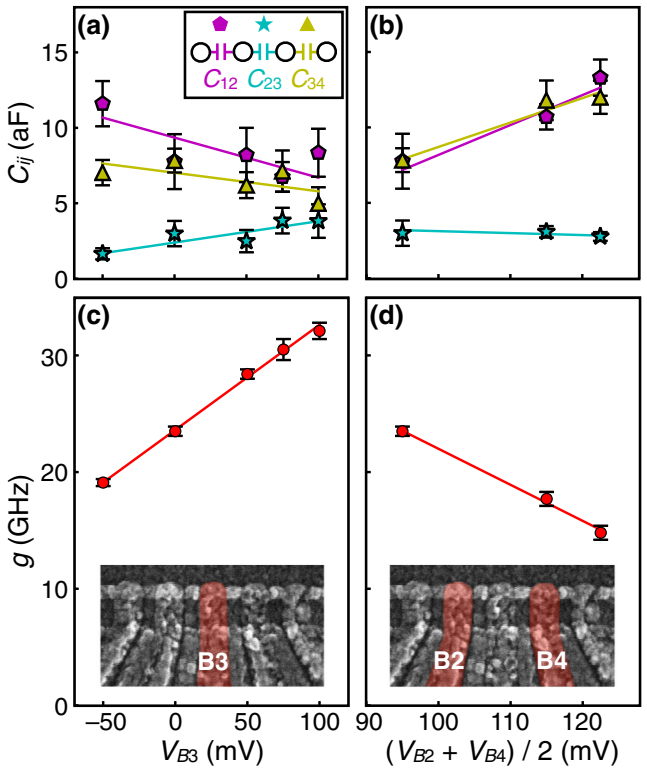


FIG. 4. (a) Interdot capacitances as a function of the middle barrier gate voltage, $V_{B3}$, with $(V_{B2}, V_{B4}) = (120, 70)$ mV. (b) Interdot capacitances as a function of the average of the two outer barrier gate voltages, $V_{B2}$ and $V_{B4}$, with $V_{B3} = 0$ mV. The gate voltage values for all points are, from left to right: $(V_{B2}, V_{B4}) = (120, 70)$, (140,90), and (155,90) mV. (c) Capacitive coupling as a function of $V_{B3}$. Inset: false-colored SEM micrograph highlighting the gate whose voltage is varied. (d) Capacitive coupling as a function of $V_{B2}$ and $V_{B4}$. Inset: false-colored SEM micrograph highlighting the gates whose voltages are varied. For all plots, linear fits to the data are shown as a guide for the eye.

we investigate the relationships among capacitive coupling, inter-DD capacitance, and intra-DD capacitances. In Figs. 4(a) and 4(c), the middle barrier voltage, $V_{B3}$, is varied with $V_{B2}$ and $V_{B4}$ held fixed. Figure 4(c) shows how increasing $V_{B3}$ increases the capacitive coupling, $g$. Figure 4(a) shows the effect of $V_{B3}$ on all the interdot capacitances in the system. Increasing $V_{B3}$ increases the inter-DD capacitance ($C_{23}$) and also decreases both intra-DD capacitances ($C_{12}$ and $C_{34}$). These changes in capacitance are a result of the position of the dots shifting in the array. Making $V_{B3}$ more positive decreases the potential between dots 2 and 3, resulting in these dots shifting closer together (increasing $C_{23}$) and farther from their outer neighbors, 1 and 4 (decreasing $C_{12}$ and $C_{34}$). The effects of these changes in gate voltage on the coupling $g$ follow the intuition for a dipole-dipole interaction, where a decrease in the spacing between the dipoles causes an increase in the interaction energy.

In Figs. 4(b) and 4(d), $V_{B3}$ is held fixed and $V_{B2}$ and $V_{B4}$ are varied. Figure 4(d) shows how increasing $V_{B2}$ and $V_{B4}$ decreases $g$. Figure 4(b) shows the effect of these barrier voltages on the interdot capacitances. Here, the change in inter-DD capacitance is small, whereas the intra-DD capacitances change significantly in response to $V_{B2}$ and $V_{B4}$. Making these voltages more positive decreases the potential in the middle of each double dot, shrinking the spacing between dots in each pair (increasing $C_{12}$ and $C_{34}$). The effects of these changes in gate voltage on the coupling $g$ again follow the intuition for a dipole-dipole interaction, where here a decrease in intra-DD spacing corresponds to a decrease in the size of the dipoles, which decreases the interaction energy.

To estimate the shift in quantum-dot positions associated with the changes in capacitance observed in Figs. 4(a) and 4(b), we model a pair of neighboring dots as two conducting disks beneath a conducting plane, which incorporates the screening effects from the overlapping gate metal [34]. We assume a dot diameter equal to the plunger gate width of 80 nm. The capacitance in this model follows an approximate $1/d^3$ dependence, where $d$ is the center-to-center distance between the dots. Varying $d$ from 85 to 175 nm, to cover the range over which this spacing could vary in an array of 80 nm dots with 130 nm gate pitch, we calculate interdot capacitances ranging from 1 to 10 aF, in good agreement with the measured capacitances in Figs. 4(a) and 4(b), which range from 2 to 13 aF. These numbers also suggest that the variations in interdot capacitance observed in Fig. 4 are the result of significant shifts in dot position, on the order of tens of nanometers, with a dot pitch on the low $C_{ij}$ end (approximately 1 aF) of around 170 nm and a dot pitch on the high $C_{ij}$ end (approximately 10 aF) of around 90 nm.

To further understand the contributions that the inter- and intra-DD capacitances make to the capacitive coupling, we model the quadruple-dot system as a network of four charge nodes joined by capacitors. The capacitive coupling creates a detuning shift in one double dot owing to the change in polarization of the other double dot. We extend the analysis from Ref. [46] from two to four quantum dots and calculate this detuning shift to obtain an analytical expression for capacitive coupling as a function of the capacitive elements shown in Fig. 1(c) (details given in the Supplemental Material [34]):

$$g = \frac{e^2}{|\mathbf{C}|} C_{23}(C_1 - C_{12})(C_4 - C_{34}) \tag{3}$$

where $e$ is the electron charge and $|\mathbf{C}|$ is the determinant of the capacitance matrix. We can simplify the expression by approximating all $C_i = C$. Then, assuming interdot capacitances are small compared with total dot capacitances, we can series expand in the ratios $c_{ij} = C_{ij}/C$, finding, to

second order,

$$g/E_C = c_{23} - c_{23}c_{12} - c_{23}c_{34}, \tag{4}$$

where $E_C = e^2/C$ is the single-dot charging energy. The approximate expression in Eq. (4) provides intuition for the relative contributions that the inter- and intra-DD capacitances make to the capacitive coupling and how the capacitive coupling should trend with each. The leading contribution of the inter-DD capacitance ($c_{23}$) is first order, whereas the leading contributions of the intra-DD capacitances ($c_{12}$ and $c_{34}$) are second order. The capacitive coupling depends positively on inter-DD capacitance but negatively on intra-DD capacitances. This agrees with the correlations we observe between interdot capacitances and capacitive coupling, as shown in Fig. 4, where changes in inter-DD (intra-DD) capacitance correlate positively (negatively) with changes in capacitive coupling.

### D. Discussion

As discussed in Sec. II A, these experiments are performed around the (3,2)-(2,3) transition with five electrons in each double dot. Many double-dot qubit experiments are performed at lower electron occupancy, with one, two, and three electrons per double dot being typical for charge qubits, singlet-triplet qubits, and QDHQs, respectively. We note that the fitting procedure demonstrated in Fig. 3 applies equally well when both double dots are in a fewer-electron regime. The electrostatics model that generates Eq. (4) does not depend on absolute charge number and assumes only that charge is quantized, i.e., that the dots are in Coulomb blockade. The capacitively mediated dipole-dipole interaction that arises from the movement of single charges does not depend explicitly on actual charge number but depends on the capacitance matrix of the system.

The results in Fig. 4 demonstrate a large degree of control over the capacitive coupling using the interdot barrier voltages to change the interdot capacitances in the array. When this device is tuned to a realistic regime for performing two-qubit experiments, where intra-DD tunnel coupling is high ($t_{12}, t_{34} > 1$ GHz) and the inter-DD tunnel coupling is very low ($t_{23} \lesssim 1$ kHz), we find a capacitive coupling of approximately 20 GHz, which corresponds to a fast two-qubit entangling time of around 20 ps when both qubits have equal admixtures of $|L\rangle$ and $|R\rangle$ states. Based on the trends observed in Fig. 4(c), if an even higher capacitive coupling rate were desired, we expect the coupling could be increased further in this device by raising $V_{B3}$ to increase $C_{23}$ while raising $V_{B2}$ and $V_{B4}$ to maintain strong intra-DD tunnel couplings. This would raise the inter-DD leakage rate across B3, but for many semiconductor qubits, this rate could be brought into the megahertz range without surpassing the operation rate of the qubits themselves. The ability to raise $C_{23}$ while keeping $t_{23}$ low could also be enhanced further by making the barrier potential between dots 2 and 3 higher and narrower, which could be achieved by a straightforward lithographic change of decreasing the gap between plunger gates P2 and P3. We note also that a proportional decrease of all distances in the dot array leads to increased values of $g$, which is consistent with the larger values of $g$ (approximately 50 GHz) that have been measured in a dot array with a smaller (100 nm) pitch [33].

When the intra-DD tunnel couplings and capacitive coupling are set to appropriate values using the approach described above, the measurement and analysis shown in Fig. 3 can provide a useful framework for setting up two-qubit gates. In the case of two coupled QDHQs, in the far detuned regime, the energies of the $|0\rangle$ and $|1\rangle$ states become close to parallel as a function of detuning $\epsilon$, giving protection from charge noise and also enabling single-qubit operations that do not depend on the state of the other QDHQ. For detunings closer to the polarization line, the QDHQ states $|0\rangle$ and $|1\rangle$ acquire slightly different charge components, and thus the QDHQ develops a charge dipole whose magnitude is tunable with $\epsilon$. When both QDHQs are tuned to the regime in which nonzero charge dipoles exist, the capacitive coupling $g$ causes the phase of the four two-qubit basis states to evolve in a manner consistent with a controlled-phase gate [45].

## III. CONCLUSION

We measure the capacitive coupling and all inter- and intra-DD capacitances in a linear array of four quantum dots in the few-electron regime at a range of tunings. We tune to a regime of strong intra-DD tunnel coupling and measure the capacitive coupling to be $g = 20.9 \pm 0.3$ GHz, which is strong enough to be able to implement high-fidelity two-qubit operations. We demonstrate a fitting procedure to extract all the parameters of the 4D Hamiltonian for two capacitively coupled charge qubits from a 2D slice through the quadruple-dot stability diagram. We tune the capacitive elements in the quadruple-dot array with interdot barrier gate voltages and see the capacitive coupling change over a range of 15–32 GHz. We provide a simple model based on a system of charge nodes joined by capacitors to illustrate how capacitive coupling should depend on the inter-DD and intra-DD capacitances of the system and find the model agrees well with the trends in the measured data.

## ACKNOWLEDGMENTS

This research was sponsored in part by the Army Research Office (ARO) under Grant No. W911NF-17-1-0274 and by the Vannevar Bush Faculty Fellowship program under ONR Grant No. N00014-15-1-0029. We acknowledge the use of facilities supported by NSF

through the UW-Madison MRSEC (Grant No. DMR-1720415). The views and conclusions contained in this document are those of the authors and should not be interpreted as representing the official policies, either expressed or implied, of the Army Research Office (ARO), or the U.S. Government. The U.S. Government is authorized to reproduce and distribute reprints for Government purposes notwithstanding any copyright notation herein.

[1] D. Loss and D. P. DiVincenzo, Quantum computation with quantum dots, Phys. Rev. A **57**, 120 (1998).
[2] Maximilian Russ and Guido Burkard, Three-electron spin qubits, J. Phys.: Condens. Matter **29**, 393001 (2017).
[3] Xin Zhang, Hai-Ou Li, Gang Cao, Ming Xiao, Guang-Can Guo, and Guo-Ping Guo, Semiconductor quantum computation, Natl. Sci. Rev. **6**, 32 (2018).
[4] F. A. Zwanenburg, A. S. Dzurak, A. Morello, M. Y. Simmons, L. C. L. Hollenberg, G. Klimeck, S. Rogge, S. N. Coppersmith, and M. A. Eriksson, Silicon quantum electronics, Rev. Mod. Phys. **85**, 961 (2013).
[5] L. J. Klein, K. A. Slinker, J. L. Truitt, S. Goswami, K. L. M. Lewis, S. N. Coppersmith, D. W. van der Weide, M. Friesen, R. H. Blick, D. E. Savage, M. G. Lagally, C. Tahan, R. Joynt, M. A. Eriksson, J. O. Chu, J. A. Ott, and P. M. Mooney, Coulomb blockade in a silicon/silicon-germanium two-dimensional electron gas quantum dot, Appl. Phys. Lett. **84**, 4047 (2004).
[6] T. M. Lu, N. C. Bishop, T. Pluym, J. Means, P. G. Kotula, J. Cederberg, L. A. Tracy, J. Dominguez, M. P. Lilly, and M. S. Carroll, Enhancement-mode buried strained silicon channel quantum dot with tunable lateral geometry, Appl. Phys. Lett. **99**, 043101 (2011).
[7] M. G. Borselli, K. Eng, E. T. Croke, B. M. Maune, B. Huang, R. S. Ross, A. A. Kiselev, P. W. Deelman, I. Alvarado-Rodriguez, A. E. Schmitz, M. Sokolich, K. S. Holabird, T. M. Hazard, M. F. Gyure, and A. T. Hunter, Pauli spin blockade in undoped Si/SiGe two-electron double quantum dots, Appl. Phys. Lett. **99**, 063109 (2011).
[8] K. Wang, C. Payette, Y. Dovzhenko, P. W. Deelman, and J. R. Petta, Charge Relaxation in a Single-Electron Si/SiGe Double Quantum Dot, Phys. Rev. Lett. **111**, 046801 (2013).
[9] Xian Wu, D. R. Ward, J. R. Prance, Dohun Kim, John King Gamble, R. T. Mohr, Zhan Shi, D. E. Savage, M. G. Lagally, Mark Friesen, S. N. Coppersmith, and M. A Eriksson, Two-axis control of singlet-triplet qubit with an integrated micromagnet, PNAS **111**, 11938 (2014).
[10] Erika Kawakami, Thibaut Jullien, Pasquale Scarlino, Daniel R. Ward, Donald E. Savage, Max G. Lagally, Viatcheslav V. Dobrovitski, Mark Friesen, Susan N. Coppersmith, Mark A. Eriksson, and Lieven M. K. Vandersypen, Gate fidelity and coherence of an electron spin in an Si/SiGe quantum dot with micromagnet, PNAS **113**, 11738 (2016).
[11] Jun Yoneda, Kenta Takeda, Tomohiro Otsuka, Takashi Nakajima, Matthieu R. Delbecq, Giles Allison, Takumu Honda, Tetsuo Kodera, Shunri Oda, Yusuke Hoshi, Noritaka Usami, Kohei M. Itoh, and Seigo Tarucha, A quantum-dot spin qubit with coherence limited by charge noise and fidelity higher than 99.9%, Nat. Nanotechnol. **13**, 102 (2018).
[12] D. M. Zajac, A. J. Sigillito, M. Russ, F. Borjans, J. M. Taylor, G. Burkard, and J. R. Petta, Resonantly driven CNOT gate for electron spins, Science **359**, 439 (2018).
[13] T. F. Watson, S. G. J. Philips, E. Kawakami, D. R. Ward, P. Scarlino, M. Veldhorst, D. E. Savage, M. G. Lagally, Mark Friesen, S. N. Coppersmith, M. A. Eriksson, and L. M. K. Vandersypen, A programmable two-qubit quantum processor in silicon, Nature **555**, 633 (2018).
[14] X. Mi, M. Benito, S. Putz, D. M. Zajac, J. M. Taylor, Guido Burkard, and J. R. Petta, A coherent spin–photon interface in silicon, Nature **555**, 599 (2018).
[15] X. Xue, T. F. Watson, J. Helsen, D. R. Ward, D. E. Savage, M. G. Lagally, S. N. Coppersmith, M. A. Eriksson, S. Wehner, and L. M. K. Vandersypen, Benchmarking Gate Fidelities in a Si/SiGe Two-Qubit Device, Phys. Rev. X **9**, 021011 (2019).
[16] B. M. Maune, M. G. Borselli, B. Huang, T. D. Ladd, P. W. Deelman, K. S. Holabird, A. A. Kiselev, I. Alvarado-Rodriguez, R. S. Ross, A. E. Schmitz, M. Sokolich, C. A. Watson, M. F. Gyure, and A. T. Hunter, Coherent singlet-triplet oscillations in a silicon-based double quantum dot, Nature **481**, 344 (2012).
[17] M. D. Reed, B. M. Maune, R. W. Andrews, M. G. Borselli, K. Eng, M. P. Jura, A. A. Kiselev, T. D. Ladd, S. T. Merkel, I. Milosavljevic, E. J. Pritchett, M. T. Rakher, R. S. Ross, A. E. Schmitz, A. Smith, J. A. Wright, M. F. Gyure, and A. T. Hunter, Reduced Sensitivity to Charge Noise in Semiconductor Spin Qubits via Symmetric Operation, Phys. Rev. Lett. **116**, 110402 (2016).
[18] Dohun Kim, Zhan Shi, C. B. Simmons, D. R. Ward, J. R. Prance, Teck Seng Koh, John King Gamble, D. E. Savage, M. G. Lagally, Mark Friesen, S. N. Coppersmith, and M. A. Eriksson, Quantum control and process tomography of a semiconductor quantum dot hybrid qubit, Nature **511**, 70 (2014).
[19] Brandur Thorgrimsson, Dohun Kim, Yuan-Chi Yang, L. W. Smith, C. B. Simmons, D. R. Ward, R. H. Foote, J. Corrigan, D. E. Savage, M. G. Lagally, Mark Friesen, S. N. Coppersmith, and M. A. Eriksson, Extending the coherence of a quantum dot hybrid qubit, npj Quantum Inf. **3**, 32 (2017).
[20] Joshua S. Schoenfield, Blake M. Freeman, and HongWen Jiang, Coherent manipulation of valley states at multiple charge configurations of a silicon quantum dot device, Nat. Commun. **8**, 64 (2017).
[21] X. Mi, S. Kohler, and J. R. Petta, Landau-Zener interferometry of valley-orbit states in Si/SiGe double quantum dots, Phys. Rev. B **98**, 161404(R) (2018).
[22] Kevin Eng, Thaddeus D. Ladd, Aaron Smith, Matthew G. Borselli, Andrey A. Kiselev, Bryan H. Fong, Kevin S. Holabird, Thomas M. Hazard, Biqin Huang, Peter W. Deelman, Ivan Milosavljevic, Adele E. Schmitz, Richard S. Ross, Mark F. Gyure, and Andrew T. Hunter, Isotopically enhanced triple-quantum-dot qubit, Sci. Adv. **1**, e1500214 (2015).
[23] K. C. Nowack, M. Shafiei, M. Laforest, G. E. D. K. Prawiroatmodjo, L. R. Schreiber, C. Reichl, W. Wegscheider, and

L. M. K. Vandersypen, Single-shot correlations and two-qubit gate of solid-state spins, Science **333**, 1269 (2011).

[24] R. Brunner, Y.-S. Shin, T. Obata, M. Pioro-Ladriere, T. Kubo, K. Yoshida, T. Taniyama, Y. Tokura, and S. Tarucha, Two-Qubit Gate of Combined Single-Spin Rotation and Interdot Spin Exchange in a Double Quantum Dot, Phys. Rev. Lett. **107**, 146801 (2011).

[25] M. Veldhorst, C. H. Yang, J. C. C. Hwang, W. Huang, J. P. Dehollain, J. T. Muhonen, S. Simmons, A. Laucht, F. E. Hudson, K. M. Itoh, A. Morello, and A. S. Dzurak, A two-qubit logic gate in silicon, Nature **526**, 410 (2015).

[26] N. W. Hendrickx, D. P. Franke, A. Sammak, G. Scappucci, and M. Veldhorst, Fast two-qubit logic with holes in germanium, arXiv:1904.11443 (2019).

[27] M. D. Shulman, O. E. Dial, S. P. Harvey, H. Bluhm, V. Umansky, and A. Yacoby, Demonstration of entanglement of electrostatically coupled singlet-triplet qubits, Science **336**, 202 (2012).

[28] John M. Nichol, Lucas A. Orona, Shannon P. Harvey, Saeed Fallahi, Geoffrey C. Gardner, Michael J. Manfra, and Amir Yacoby, High-fidelity entangling gate for double-quantum-dot spin qubits, npj Quantum Inf. **3**, 1 (2017).

[29] H.-O. Li, G. Cao, G.-D. Yu, M. Xiao, G.-C. Guo, H.-W. Jiang, and G.-P. Guo, Conditional rotation of two strongly coupled semiconductor charge qubits, Nat. Commun. **6**, 7681 (2015).

[30] I. van Weperen, B. D. Armstrong, E. A. Laird, J. Medford, C. M. Marcus, M. P. Hanson, and A. C. Gossard, Charge-State Conditional Operation of a Spin Qubit, Phys. Rev. Lett. **107**, 030506 (2011).

[31] Guo-Dong Yu, Hai-Ou Li, Gang Cao, Ming Xiao, Hong-Wen Jiang, and Guo-Ping Guo, Tunable capacitive coupling between two semiconductor charge qubits, Nanotechnology **27**, 324003 (2016).

[32] Daniel R. Ward, Dohun Kim, Donald E. Savage, Max G. Lagally, Ryan H. Foote, Mark Friesen, Susan N. Coppersmith, and Mark A. Eriksson, State-conditional coherent charge qubit oscillations in a Si/SiGe quadruple quantum dot, npj Quantum Inf. **2**, 16032 (2016).

[33] D. M. Zajac, T. M. Hazard, X. Mi, E. Nielsen, and J. R. Petta, Scalable Gate Architecture for a One-Dimensional Array of Semiconductor Spin Qubits, Phys. Rev. Appl. **6**, 054013 (2016).

[34] See Supplemental Material at http://link.aps.org/supplemental/10.1103/PhysRevApplied.12.064049 for more discussion of the fabrication process, measurements of the lever arms, fits for the Hamiltonian parameters, measurements and modeling of the inter-dot capacitances, and the derivation of the analytical expression for $g$.

[35] P. W. Deelman, L. F. Edge, and C. A. Jackson, Metamorphic materials for quantum computing, Mater. Res. Bull. **41**, 224 (2016).

[36] C. J. K. Richardson, C. A. Jackson, L. F. Edge, and P. W. Deelman, High-resolution x-ray reflection Fourier analysis of metamorphic Si/SiGe quantum wells, J. Vac. Sci. Technol. B **35**, 02B113 (2017).

[37] L. A. Tracy, D. R. Luhman, S. M. Carr, N. C. Bishop, G. A. Ten Eyck, T. Pluym, J. R. Wendt, M. P. Lilly, and M. S. Carroll, Single shot spin readout using a cryogenic high-electron-mobility transistor amplifier at sub-Kelvin temperatures, Appl. Phys. Lett. **108**, 063101 (2016).

[38] L. DiCarlo, H. J. Lynch, A. C. Johnson, L. I. Childress, K. Crockett, C. M. Marcus, M. P. Hanson, and A. C. Gossard, Differential Charge Sensing and Charge Delocalization in a Tunable Double Quantum Dot, Phys. Rev. Lett. **92**, 226801 (2004).

[39] C. B. Simmons, M. Thalakulam, B. M. Rosemeyer, B. J. Van Bael, E. K. Sackmann, D. E. Savage, M. G. Lagally, R. Joynt, M. Friesen, S. N. Coppersmith, and M. A. Eriksson, Charge sensing and controllable tunnel coupling in a Si/SiGe double quantum dot, Nano Lett. **9**, 3234 (2009).

[40] Y. Nazarov and Y. Blanter, *Quantum Transport: Introduction to Nanoscience*, 1st ed. (Cambridge University Press, New York, 2009).

[41] K. D. Petersson, J. R. Petta, H. Lu, and A. C. Gossard, Quantum Coherence in a One-Electron Semiconductor Charge Qubit, Phys. Rev. Lett. **105**, 246804 (2010).

[42] Zhan Shi, C. B. Simmons, Daniel R. Ward, J. R. Prance, R. T. Mohr, Teck Seng Koh, John King Gamble, Xian Wu, D. E. Savage, M. G. Lagally, Mark Friesen, S. N. Coppersmith, and M. A. Eriksson, Coherent quantum oscillations and echo measurements of a Si charge qubit, Phys. Rev. B **88**, 075416 (2013).

[43] Dohun Kim, D. R. Ward, C. B. Simmons, John King Gamble, Robin Blume-Kohout, Erik Nielsen, D. E. Savage, M. G. Lagally, Mark Friesen, S. N. Coppersmith, and M. A. Eriksson, Microwave-driven coherent operations of a semiconductor quantum dot charge qubit, Nat. Nanotechnol. **10**, 243 (2015).

[44] Gang Cao, Hai-Ou Li Guo-Dong Yu, Bao-Chuan Wang, Bao-Bao Chen, Xiang-Xiang Song, Ming Xiao, Guang-Can Guo, Hong-Wen Jiang, Xuedong Hu, and Guo-Ping Guo, Tunable Hybrid Qubit in a GaAs Double Quantum Dot, Phys. Rev. Lett. **116**, 086801 (2016).

[45] Adam Frees, Sebastian Mehl, John King Gamble, Mark Friesen, and S. N. Coppersmith, Adiabatic two-qubit gates in capacitively coupled quantum dot hybrid qubits, npj Quantum Inf. **5**, 73 (2019).

[46] W. G. van der Wiel, S. De Franceschi, J. M. Elzerman, T. Fujisawa, S. Tarucha, and L. P. Kouwenhoven, Electron transport through double quantum dots, Rev. Mod. Phys. **75**, 1 (2003).